Research Article | Vol. 28, No. 14 / 6 July 2020 / Optics Express 20296
Optics EXPRESS

Ultrafast modulation of the spectral filtering properties of a THz metasurface

LAUREN GINGRAS,[1] AHMED JABER,[1] ALI MALEKI,[1] ORAD RESHEF,[1] KSENIA DOLGALEVA,[1,2] ROBERT W. BOYD,[1,2,3] AND JEAN-MICHEL MÉNARD[1,*]

[1] *Physics Department, University of Ottawa, 25 Templeton St., Ottawa, ON K1N 6N5, Canada*
[2] *School of Electrical Engineering and Computer Science, University of Ottawa, 25 Templeton St., Ottawa, ON K1N 6N5, Canada*
[3] *Institute of Optics and Department of Physics and Astronomy, University of Rochester, Rochester, New York 14627, USA*
[*] *jean-michel.menard@uottawa.ca*

Abstract: We demonstrate ultrafast tuning of a plasmonic spectral filter at terahertz (THz) frequencies. The device is made of periodically spaced gold crosses deposited on the surface of an undoped silicon wafer in which transient free carriers can be optically injected with a femtosecond resonant pulse. We demonstrate the concept by measuring the transmission spectrum of a notch filter using time-domain THz spectroscopy. Proper synchronization of the THz probe and visible excitation pulses leads to an enhanced transmission at the resonance by more than two orders of magnitude. Finite-difference time-domain simulations, which are in agreement with the experimental results, show that the underlying mechanisms responsible for the resonance blueshift and linewidth broadening can be attributed to the photoinduced change in dielectric properties of the substrate. This is supported by the numerically simulated field distribution and reflection/transmission coefficients. The device can be used in future pulse shaping and ultrafast switching experiments.

1. Introduction

Metamaterials present new avenues to control light in ways otherwise not accessible in conventional materials. As such, engineered metasurfaces have led to the observation of novel phenomena such as negative refraction [1–3], metalensing [4,5], and invisibility cloaking [6]. Theoretically predicted effects such as Fano-type resonances [7–10] as well as magneto-optically induced transparency [11,12] have also been achieved in the terahertz (THz) spectral range using carefully engineered metamaterials. Thanks to their relatively small footprint and high flexibility, THz metasurfaces have attracted recent attention because of their promising applications in sensing and imaging [13,14]. Other THz components, such as metalenses [15,16], waveplates [17,18] and phase modulators [19], have also been demonstrated alongside control over the polarization state [20] and beam pointing [21].

Tunability is obviously a very desirable function of metasurfaces as it lends itself to more practical applications. Amongst the modulation methods demonstrated, electrically gated materials [22–24] and MEMS [25] have leveraged industry standard methods to tune the effective dielectric properties of a metasurface. Notable demonstrations also include mechanical tuning [26], permeability tuning [27], as well as approaches leveraging the insulator-to-metal transitions of VO_2 [28,29]. The major drawback with most of the aforementioned methods is that they rely on slow mechanisms to achieve tuning of the metasurfaces. One way to circumvent this limitation is to employ optical switching, which can be done in a sub-picosecond manner using femtosecond pulsed laser sources [30,31].

#395508 https://doi.org/10.1364/OE.395508
Journal © 2020 Received 17 Apr 2020; revised 10 Jun 2020; accepted 11 Jun 2020; published 24 Jun 2020

Optics EXPRESS

Split ring resonators (SRRs) have perhaps seen the greatest interest at THz frequencies since the demonstration of active tuning [23,32] and of perfectly absorbing resonances [33]. The magnetic nature of most SSR designs grants more tunability over the effective dielectric parameters of the metasurface though it may limit their functionality to only one polarization state. Cross resonators, on the other hand, offer a purely electric response [34,35] and exhibit no polarization anisotropy given the 4-fold symmetry of their unit cell. These structures have already been used to demonstrate spatial and frequency selective transmission [36] and optical tunability on high-temperature superconducting resonators [37].

In this work, we demonstrate, for the first time, the ability to tune a notch filter made from a purely electric THz metasurface comprised of an array of metal crosses deposited atop silicon. Using THz time-domain spectroscopy, we show that the engineered resonance can be blueshifted and bleached by the photo-induction of free charge carriers. More importantly, this technique can be used to increase the transmission of the spectral component at the notch filter's resonance frequency by more than two orders of magnitude. We examine the relevant functional characteristics of the metasurface and discuss the nature of the observed blueshifted resonance. Finite-difference time-domain (FDTD) simulations, in good agreement with experimental results, are used to support a discussion on free-carrier-induced changes in the center frequency and linewidth of the spectral resonance.

2. Experimental methods

We use time-domain THz spectroscopy to monitor the optical properties of the metamaterial [38]. The setup relies on an optical amplifier delivering 180 fs pulses at a wavelength of 1030 nm.

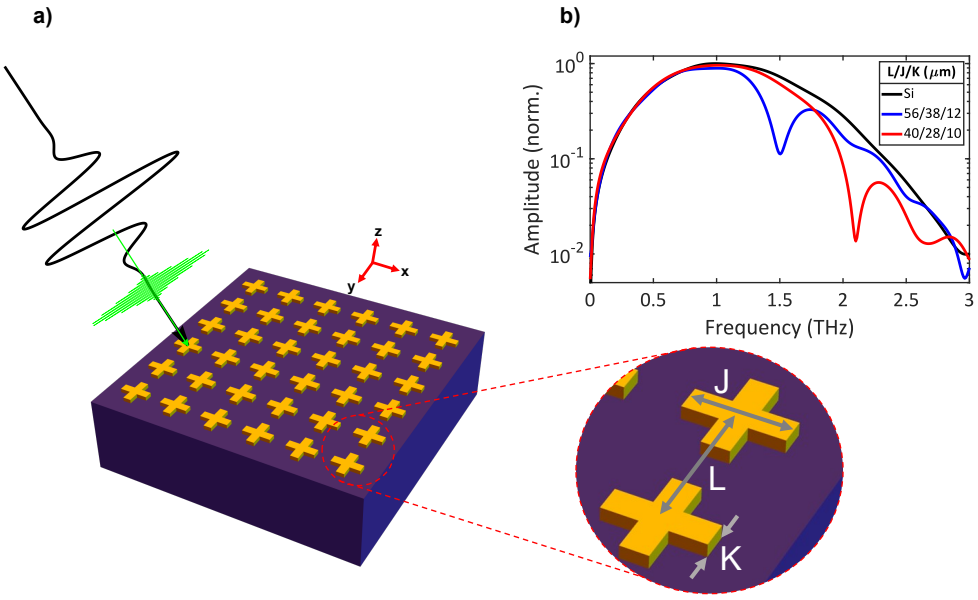

Fig. 1. (a) Schematic representation of the THz pump-probe experiment. An array of 200 nm thick gold (yellow) crosses is deposited on a 0.9 mm thick silicon substrate. The semiconductor is pumped using a visible (green) femtosecond pulse and probed using a broadband THz pulse (black). The lattice pitch (L), arm length (J) and arm thickness (K) are labelled with grey arrows. (b) Experimental transmitted spectra measured for a bare Si substrate (Si) and notch filters with resonances at 1.5 THz (L/J/K = 56/38/12 μm) and 2.1 THz (L/J/K = 40/28/10 μm).

Optics EXPRESS

Optical rectification in a 2 mm GaP crystal is used to generate single-cycle THz pulses, which are detected by electro-optical sampling inside an equally thick GaP crystal. A schematic of the metamaterial filter is shown in Fig. 1(a). A metal lift-off process is used to produce a periodic surface array of 200 nm thick gold crosses. The pattern is defined using photolithography in a positive-tone resin, and the gold is deposited onto a 0.9 mm thick float-zone silicon substrate using electron-beam evaporation. The surface plasmon resonance frequency is determined by the lattice pitch (L), cross length (J) and arm thickness (K), indicated in Fig. 1(b). We use two filter designs with characteristic dimensions (L/J/K) corresponding to a transmission dip at 1.5 THz (56/38/12 µm) and 2.1 THz (40/28/10 µm). These two measured transmission spectra are shown in Fig. 1(b) alongside with a reference measurement (black curve) corresponding to the THz transmission through the bare Si substrate. Note a proper time-windowing of the detected THz waveform allows us to remove Fabry-Perot effects [39]. Weak modulations in the transmission spectrum at frequencies higher than the main transmission dip are caused by scattering into higher-order lattice and cross-resonant modes.

The metamaterial properties are modulated with a pump pulse at a wavelength of 515 nm, obtained from the second harmonic generation of our ultrafast source. The spot size of the visible beam (~2 mm) provides uniform excitation across the focused THz beam (< 1 mm), impinging at normal incidence on the 10 mm wide metasurface. We use this pump wavelength to access a high-absorption spectral region in Si, corresponding to a short penetration depth of 1 µm, which ensures an optimal interaction between the photoinduced plasma and the THz electro-magnetic field. Finally, the laser is operated at a 6 kHz repetition rate to ensure that photoinjected electrons and holes are given enough time to recombine between successive pulses [40,41].

3. Results and discussion

The experimental results for the optically modulated transmission of the cross-mesh resonator are presented in Fig. 2(a). In this experiment, the sample is optically pumped by the visible excitation pulse 100 ps prior to the THz probe pulse arrival at the metasurface in order to avoid dynamic modulation effects. As we increase the pump intensity, we observe a dramatic increase in transmission at the resonance frequency. We calculate the transmission T of the metasurface from the measured incident and transmitted spectral amplitude, $T = E^2_{\text{trans}}/E^2_{\text{inc}}$, and normalize it by the transmission spectrum measured through the unpumped bare silicon substrate $T_{\text{bare - Si}}$ to obtain $T_{\text{norm}} = T/T_{\text{bare - Si}}$. When the sample is unpumped, we observe a prominent spectral dip at the plasmonic resonance ν_{res} corresponding to $T_{\text{norm}}(\nu_{\text{res}}) = 0.02$. As we increase the excitation pump energy, $T_{\text{norm}}(\nu_{\text{res}})$ rises by an order of magnitude, see Fig. 2(c). At an excitation pulse energy of 0.47 µJ, the injected carrier density of 2.5×10^{17} cm^{-3} bleaches the resonance dip and flattens the overall transmission spectrum such that $T_{\text{norm}} \approx 0.25$ across the full spectrum. The value of the transmission away from the resonance is then reduced by a factor of 4 due to free-carrier absorption in the semiconductor. Figure 2(b) shows the corresponding transmission plots obtained through finite-difference time-domain method (FDTD) simulations for equivalent charge carrier densities. We observe a good agreement between simulations and experimental results, especially at low carrier densities. The steep increase in the simulated transmission spectra on the high-frequency side of the resonance is caused by the first-order diffraction of the periodically structured metasurface, which is not collected in the experiment due to its high diffraction angle. Numerical simulations are described in more detail at the end of the discussion section.

The experimental and simulated transmission data sets are fitted to Lorentzians, which allow us to extract significant parameters such as the center frequency and linewidth, with an accuracy approaching few GHz. The parameters thus obtained are presented in Figs. 2(d) and (e), respectively, up to an optical pump energy of 0.18 µJ. This pump energy corresponds to an injected carrier density of 1.2×10^{17} cm^{-3} at which the resonance is then strongly bleached and

Optics EXPRESS

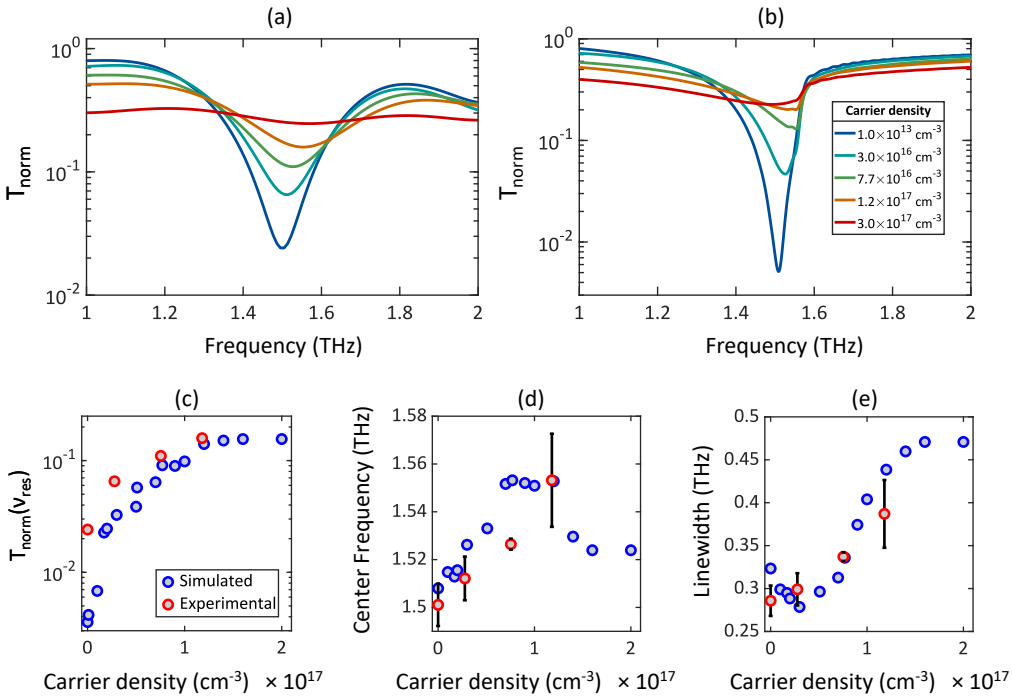

Fig. 2. (a) Normalized THz transmission T_{norm} experimentally recorded near the resonance for various pump energies. (b) Numerical simulation results for the normalized THz transmission with carrier densities matching the experimental parameters. (c) Resonant normalized THz transmission, (d) center frequency and (e) linewidth extracted from Lorentzian fits of the experimental (red circles) and simulation (blue circles) results.

can less reliably be fitted to a Lorentzian. We can see that the resonance frequency blueshifts from 1.50 to 1.55 THz with a simultaneous linewidth broadening from 0.28 to 0.39 THz, lowering the Q-factor from an initial value of 5.3, when the metasurface is unpumped, to 4.0 when we photo-inject a carrier density of 1.2×10^{17} cm^{-3}. The blueshift in resonance can be attributed to a change in the real part of the refractive index n within the thin active region of the substrate. Optically injected free carriers lower n, which decreases the effective optical path length between the gold crosses, effectively reducing the lattice pitch [42]. As a result, the plasmonic resonance, corresponding to the observed dip in transmission, shifts to shorter wavelengths (or to higher frequencies). The linewidth broadening is related to the higher Drude optical absorption, reducing the plasmonic mode lifetime. Experiments and simulations demonstrated that further increasing the carrier densities simply enhanced free-carrier absorption across the experimental spectrum (not shown here).

The pulsed nature of the optical pump used in the experiments allows us to control the relative injection time of the carriers and tune the resonance dampening in a dynamic fashion. Figure 3(a) shows THz transients of various arrival times of the 1 μJ pump relative to the THz probe for a 2.1 THz resonant metasurface. The labels refer to the pump-probe time delay t_{pp}, where $t_{\text{pp}} = 0$ ps is defined as the temporal overlap between the peak of the THz transient and the excitation 180 fs pulse. Positive times refer to an excitation pulse arriving after the peak of the THz transient. For reference, all data in Fig. 2 corresponds to $t_{\text{pp}} = -100$ ps. Here we investigate the effect of photo-injected carriers when the excitation pulse impinges on the metasurface shortly before or after the THz probe pulse. Interestingly, when t_{pp} is between 0 and 1 ps, the pump suppresses any reminiscent field oscillations in the metasurface. Therefore, spectral resonances are partially or

Optics EXPRESS

entirely suppressed in the transmission spectrum (Fig. 3(b)). This ultrafast switching mechanism allows us to increase the transmitted intensity of a THz spectral component by two orders of magnitude and simultaneously decrease the transmission at the off-resonant portion of the spectrum.

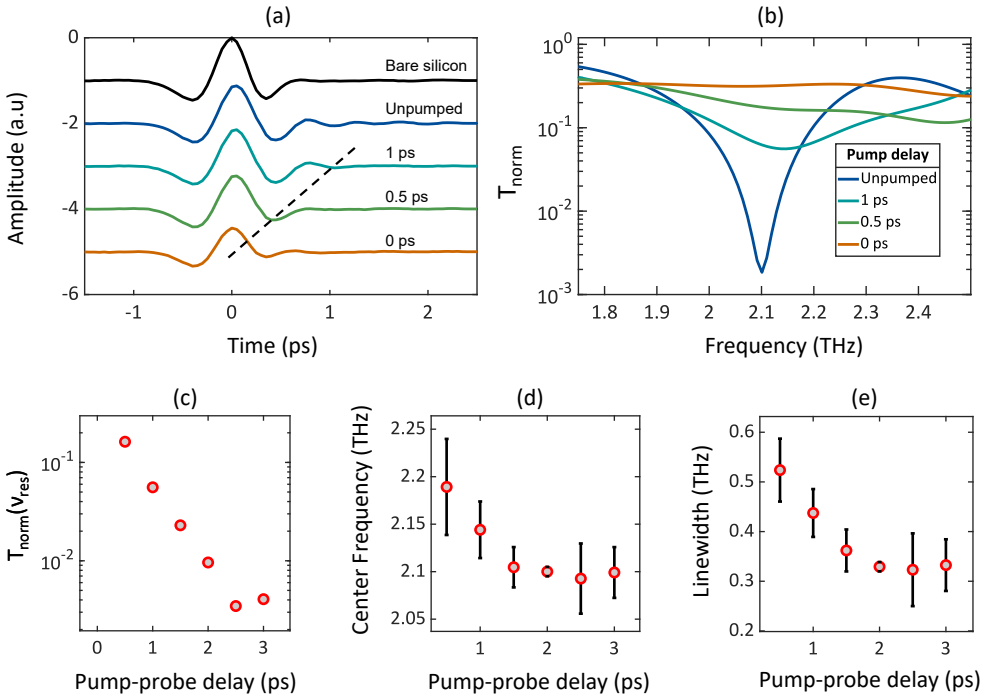

Fig. 3. (a) Experimentally measured THz transients for various pump-probe time delays with constant 1 μJ pump energy, offset for clarity. The dashed line shows the pump arrival time. (b) Associated transmission in the vicinity of the 2.1 THz resonance referenced to the transmission of the bare substrate (Si). (c) Center frequency, (d) modulation depth and (e) linewidth extracted from a Lorentzian fit to the transmission data measured at a different pump-probe time delay.

The resonance profiles are fitted to a Lorentzian lineshape to extract the center-frequency and linewidth plotted in Fig. 3(d) and (e), respectively. For a pump-probe time delay change from $t_{pp} = 3$ ps to 0.5 ps, we observe a blueshift in the center frequency from 2.10 to 2.19 THz and a linewidth broadening from 0.33 to 0.52 THz, respectively. The slight increase in the linewidth can be related to a decrease of the Q-factor, which is 6.3 in the absence of optical doping and 4.2 when $t_{pp} = 0.5$ ps.

We use three-dimensional finite-difference time-domain (FDTD) to simulate the spectral response of our notch filters and study their spatial field distribution. Periodic boundary conditions are imposed along the x and y axes for computational efficiency, a perfectly matching boundary is set along the Z direction and a 3D conductivity material model is used for gold [43] and silicon [44]. The modeled gold crosses have corners rounded to a 3 μm radius to better reproduce the device. We model the photoinjection of carriers at the surface with a multilayer stack of doped silicon with doping concentrations exponentially decaying away from the silicon surface. Peak carrier densities up to 10^{18} cm^{-3} were investigated with dielectric permittivity components defined by the Drude model. We further incorporated a frequency-dependent scattering time from the model derived by Meng *et al.* [45].

Optics EXPRESS

Figure 4 shows the time-averaged electric field distribution in the *x*-*y* plane for three different carrier concentrations in Si: undoped, 2×10^{17} cm^{-3} and 5×10^{17} cm^{-3}. The field is normalized by the time-averaged field calculated with a plain undoped Si substrate (no metallic metasurface). As such, it can be related to a local field enhancement factor. Figures 4(a)–(c) show the field distribution 100 nm above the Si substrate, which is in the center of the gold film, while Figs. 4(e)–(g) illustrate the distribution within the substrate, 500 nm below the Air-Si surface. The dimensions of the metasurface shown here correspond to the design yielding a plasmonic resonance at 2.1 THz. We see that the field enhancement, reaching one order of magnitude, is mainly localized at the outer edges of the cross' horizontal arm, the one parallel to the electric field polarization. Interestingly, we note that the spatial field localization is well represented by a decreasing exponential with a similar decay rate for all carrier densities. This is illustrated in Figs. 4(d) and (h) where the simulated electric field intensity (circles) is plotted for various carrier densities along y = 0 and fitted to an exponential decay (solid lines). The lack of appreciable change in decay rate, within uncertainty, shows that delocalization of the mode is not the dominant mechanism responsible for the disappearance of the resonance at high carrier densities. However, as the carrier density is increased to 5×10^{17} cm^{-3}, the maximum field enhancement decreases by a factor of ~2.5 both above and below the silicon surface.

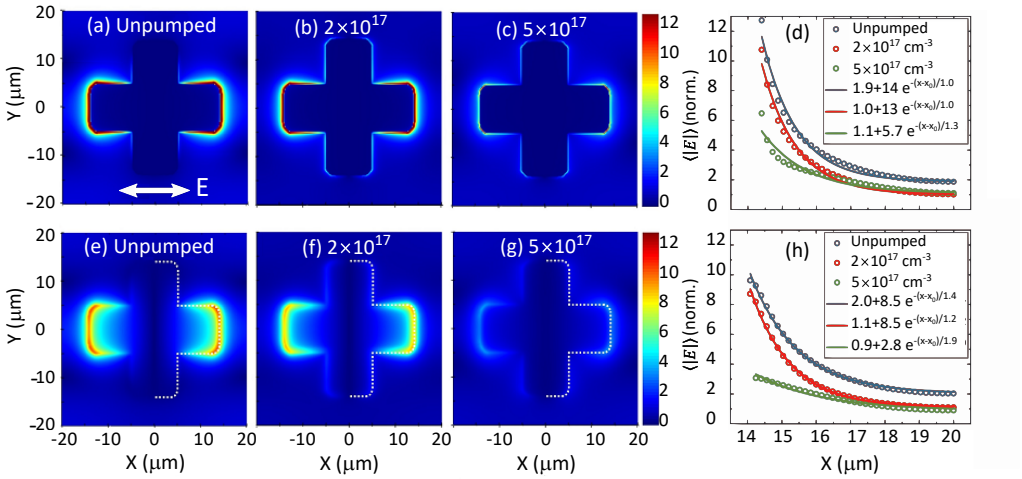

Fig. 4. In-plane spatial distribution of the time-averaged electric field amplitude at the resonance frequency at the z position corresponding to (a-c) 100 nm above the air-silicon interface, in the middle of the gold film, and (e-g) 500 nm inside the silicon, beneath the metasurface. Columns correspond to different carrier concentrations at the surface of Si: (a, e) undoped, (b, f) $2{\times}10^{17}$ cm^{-3} and (c, g) 5×10^{17} cm^{-3}. The dotted white lines show the metallic cross outline, plotted on the right half for clarity. Along the line y = 0, the resonant electric field intensity decays away in x from the gold cross edge at $x_0 = 14$ μm, (d) 100 nm above and (h) 500 nm below the Si surface. The circles show the values extracted from the simulated electric field distribution, and the solid curves are exponential fits. The field is normalized by the corresponding time-averaged field calculated with a plain undoped Si substrate.

The FDTD simulations can also be used to extract reflected the THz radiation of the investigated structures. Figures 5(a) and (b) show the simulated transmission and reflection coefficients, normalized by the time-averaged field calculated with a plain undoped Si substrate (no metallic metasurface). We can thus investigate the macroscopic optical properties of the system by looking at its transmission (T_{norm}), reflection (R_{norm}), and absorption ($1 - T_{norm} - R_{norm}$). Figure 5(a) shows the transmitted signal with a distinct minimum at the resonance frequency, which increases

Optics EXPRESS

monotonically with the free carrier density in the substrate. The reflection spectrum around the resonance, as shown in Fig. 5(b), closely follows the inverse shape of the transmission spectrum. As the carrier density increases, we observe a decrease of the reflected signal at 2.1 THz accompanied by a slight spectral broadening. Simultaneously, the absorption increases at the resonance frequency and at lower frequencies, as shown in Fig. 5(c). This increase in low-frequency absorption is consistent with the increase in loss described by Drude absorption in the presence of free carriers. Interestingly, the broadening of the notch filter spectral linewidth combined with a larger optical absorption at the resonance frequency is commensurate with an increasingly damped harmonic oscillator.

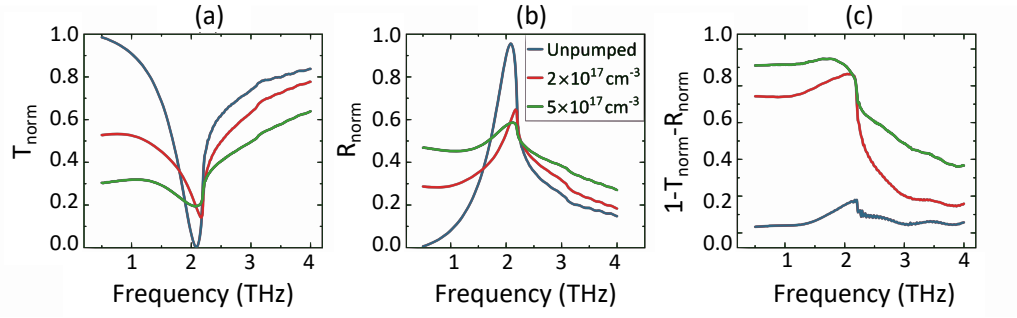

Fig. 5. (a) Transmission (T_{norm}), (b) reflection (R_{norm}), and (c) absorption ($1-T_{norm}-R_{norm}$) for a 2.1 THz resonant metasurface extracted from FDTD simulations for various charge carrier densities and normalized to bare Silicon.

4. Conclusion

We have demonstrated the ability to control the resonance of a THz metasurface notch filter. Using a visible pump-THz probe scheme, we are able to modulate the transmission at a given frequency while leaving the rest of the spectrum relatively unaffected. Most notably, we performed ultrafast re-profiling of the THz transient allowing us to increase the transmission by two orders of magnitude at the resonance frequency. The small blueshift observed in the center frequency is induced by the change in the real part of the refractive index effectively changing the lattice pitch, while the linewidth broadening is associated with the increase in Drude absorption. These features are well reproduced by simulations, which also revealed a consistent field distribution around the cross-mesh structure and low optical losses ($< 20\%$) in the system. Finally, this work paves the way for switching devices in the THz range which could rely on other substrates with shorter carrier recombination times, such as GaAs, to achieve faster switching rates. One can also envision working with a series of these structures and excitation pulses to achieve complex THz pulse structuring [46,47].

Funding

Natural Sciences and Engineering Research Council of Canada (Canada Research Chairs program, Discovery, Strategic Partnertship Grant); Canada Foundation for Innovation (Project number 35269); Office of Naval Research (N00014-19-1-2247).

Acknowledgments

The authors are thankful to Yongbao Xin, Brian Sullivan, Travis Schoepp and Graham Carlow, from Iridian Spectral Technologies for insightful discussions and fabrication of the samples.

Optics EXPRESS

Disclosures

The authors declare that there are no conflicts of interest related to this article.

References

1. J. B. Pendry, "Negative refraction makes a perfect lens," Phys. Rev. Lett. **85**(18), 3966–3969 (2000).
2. R. A. Shelby, D. R. Smith, and S. Schultz, "Experimental verification of a negative index of refraction," Science **292**(5514), 77–79 (2001).
3. S. Zhang, W. Fan, N. C. Panoiu, K. J. Malloy, R. M. Osgood, and S. R. Brueck, "Experimental demonstration of near-infrared negative-index metamaterials," Phys. Rev. Lett. **95**(13), 137404 (2005).
4. M. Khorasaninejad and F. Capasso, "Metalenses: Versatile multifunctional photonic components," Science **358**(6367), eaam8100 (2017).
5. Y. Zhou, H. Zheng, I. I. Kravchenko, and J. Valentine, "Flat optics for image differentiation," Nat. Photonics **14**(5), 316–323 (2020).
6. W. Cai, U. K. Chettiar, A. V. Kildishev, and V. M. Shalaev, "Optical cloaking with metamaterials," Nat. Photonics **1**(4), 224–227 (2007).
7. R. Singh, I. A. I. Al-Naib, M. Koch, and W. Zhang, "Sharp Fano resonances in THz metamaterials," Opt. Express **19**(7), 6312–6319 (2011).
8. M. Manjappa, Y. K. Srivastava, L. Cong, I. Al-Naib, and R. Singh, "Active Photoswitching of Sharp Fano Resonances in THz Metadevices," Adv. Mater. **29**(3), 1603355 (2017).
9. W. X. Lim, M. Manjappa, Y. K. Srivastava, L. Cong, A. Kumar, K. F. MacDonald, and R. Singh, "Ultrafast All-Optical Switching of Germanium-Based Flexible Metaphotonic Devices," Adv. Mater. **30**(9), 1705331 (2018).
10. A. Kumar, A. Solanki, M. Manjappa, S. Ramesh, Y. K. Srivastava, P. Agarwal, T. C. Sum, and R. Singh, "Excitons in 2D perovskites for ultrafast terahertz photonic devices," Sci. Adv. **6**(8), eaax8821 (2020).
11. S. Y. Chiam, R. Singh, C. Rockstuhl, F. Lederer, W. Zhang, and A. A. Bettiol, "Analogue of electromagnetically induced transparency in a terahertz metamaterial," Phys. Rev. B **80**(15), 153103 (2009).
12. J. Gu, R. Singh, X. Liu, X. Zhang, Y. Ma, S. Zhang, S. A. Maier, Z. Tian, A. K. Azad, H. T. Chen, A. J. Taylor, J. Han, and W. Zhang, "Active control of electromagnetically induced transparency analogue in terahertz metamaterials," Nat. Commun. **3**(1), 1151 (2012).
13. W. Xu, L. Xie, and Y. Ying, "Mechanisms and applications of terahertz metamaterial sensing: A review," Nanoscale **9**(37), 13864–13878 (2017).
14. K. Fan, J. Y. Suen, X. Liu, and W. J. Padilla, "All-dielectric metasurface absorbers for uncooled terahertz imaging," Optica **4**(6), 601–604 (2017).
15. J. Neu, B. Krolla, O. Paul, B. Reinhard, R. Beigang, and M. Rahm, "Metamaterial-based gradient index lens with strong focusing in the THz frequency range," Opt. Express **18**(26), 27748–27757 (2010).
16. Q. Yang, J. Gu, D. Wang, X. Zhang, Z. Tian, C. Ouyang, R. Singh, J. Han, and W. Zhang, "Efficient flat metasurface lens for terahertz imaging," Opt. Express **22**(21), 25931–25939 (2014).
17. L. Cong, N. Xu, J. Gu, R. Singh, J. Han, and W. Zhang, "Highly flexible broadband terahertz metamaterial quarter-wave plate," Laser Photonics Rev. **8**(4), 626–632 (2014).
18. V. Torres, N. Sánchez, D. Etayo, R. Ortuño, M. Navarro-Cía, A. Martínez, and M. Beruete, "Compact Dual-Band Terahertz Quarter-Wave Plate Metasurface," IEEE Photonics Technol. Lett. **26**(16), 1679–1682 (2014).
19. H.-T. Chen, W. J. Padilla, M. J. Cich, A. K. Azad, R. D. Averitt, and A. J. Taylor, "A metamaterial solid-state terahertz phase modulator," Nat. Photonics **3**(3), 148–151 (2009).
20. L. Cong, W. Cao, Z. Tian, J. Gu, J. Han, and W. Zhang, "Manipulating polarization states of terahertz radiation using metamaterials," New J. Phys. **14**(11), 115013 (2012).
21. M. R. M. Hashemi, S.-H. Yang, T. Wang, N. Sepúlveda, and M. Jarrahi, "Electronically-Controlled Beam-Steering through Vanadium Dioxide Metasurfaces," Sci. Rep. **6**(1), 35439 (2016).
22. N. Karl, K. Reichel, H.-T. Chen, A. J. Taylor, I. Brener, A. Benz, J. L. Reno, R. Mendis, and D. M. Mittleman, "An electrically driven terahertz metamaterial diffractive modulator with more than 20 dB of dynamic range," Appl. Phys. Lett. **104**(9), 091115 (2014).
23. H.-T. Chen, W. J. Padilla, J. M. O. Zide, A. C. Gossard, A. J. Taylor, and R. D. Averitt, "Active terahertz metamaterial devices," Nature **444**(7119), 597–600 (2006).
24. F. Ma, Y. S. Lin, X. Zhang, and C. Lee, "Tunable multiband terahertz metamaterials using a reconfigurable electric split-ring resonator array," Light: Sci. Appl. **3**(5), e171 (2014).
25. Z. Han, K. Kohno, H. Fujita, K. Hirakawa, and H. Toshiyoshi, "MEMS reconfigurable metamaterial for terahertz switchable filter and modulator," Opt. Express **22**(18), 21326–21339 (2014).
26. J. Li, C. M. Shah, W. Withayachumnankul, B. S.-Y. Ung, A. Mitchell, S. Sriram, M. Bhaskaran, S. Chang, and D. Abbott, "Mechanically tunable terahertz metamaterials," Appl. Phys. Lett. **102**(12), 121101 (2013).
27. J. Pendry, A. Holden, D. Robbins, and W. Stewart, "Magnetism from conductors and enhanced nonlinear phenomena," IEEE Trans. Microwave Theory Tech. **47**(11), 2075–2084 (1999).
28. T. Driscoll, H.-T. Kim, B.-G. Chae, B.-J. Kim, Y.-W. Lee, N. M. Jokerst, S. Palit, D. R. Smith, M. Di Ventra, and D. N. Basov, "Memory Metamaterials," Science **325**(5947), 1518–1521 (2009).

Optics EXPRESS

29. M. Seo, J. Kyoung, H. Park, S. Koo, H.-S. Kim, H. Bernien, B. J. Kim, J. H. Choe, Y. H. Ahn, H.-T. Kim, N. Park, Q.-H. Park, K. Ahn, and D.-S. Kim, "Active Terahertz Nanoantennas Based on VO2 Phase Transition," Nano Lett. **10**(6), 2064–2068 (2010).
30. H.-T. Chen, W. J. Padilla, J. M. O. Zide, S. R. Bank, A. C. Gossard, A. J. Taylor, and R. D. Averitt, "Ultrafast optical switching of terahertz metamaterials fabricated on ErAs/GaAs nanoisland superlattices," Opt. Lett. **32**(12), 1620–1622 (2007).
31. Y. Yang, N. Kamaraju, S. Campione, S. Liu, J. L. Reno, M. B. Sinclair, R. P. Prasankumar, and I. Brener, "Transient GaAs Plasmonic Metasurfaces at Terahertz Frequencies," ACS Photonics **4**(1), 15–21 (2017).
32. H. T. Chen, J. F. O'Hara, A. K. Azad, A. J. Taylor, R. D. Averitt, D. B. Shrekenhamer, and W. J. Padilla, "Experimental demonstration of frequency-agile terahertz metamaterials," Nat. Photonics **2**(5), 295–298 (2008).
33. N. I. Landy, S. Sajuyigbe, J. J. Mock, D. R. Smith, and W. J. Padilla, "Perfect metamaterial absorber," Phys. Rev. Lett. **100**(20), 207402 (2008).
34. D. W. Porterfield, J. L. Hesler, R. Densing, E. R. Mueller, T. W. Crowe, and R. M. Weikle, "Resonant metal-mesh bandpass filters for the far infrared," Appl. Opt. **33**(25), 6046–6052 (1994).
35. A. M. Melo, M. A. Kornberg, P. Kaufmann, M. H. Piazzetta, E. C. Bortolucci, M. B. Zakia, O. H. Bauer, A. Poglitsch, and A. M. Da Silva, "Metal mesh resonant filters for terahertz frequencies," Appl. Opt. **47**(32), 6064–6069 (2008).
36. X. Liu, T. Starr, A. F. Starr, and W. J. Padilla, "Infrared spatial and frequency selective metamaterial with near-unity absorbance," Phys. Rev. Lett. **104**(20), 207403 (2010).
37. R. Singh, J. Xiong, A. K. Azad, H. Yang, S. A. Trugman, Q. X. Jia, A. J. Taylor, and H. T. Chen, "Optical tuning and ultrafast dynamics of high-temperature superconducting terahertz metamaterials," Nanophotonics **1**(1), 117–123 (2012).
38. X.-C. Zhang and J. Xu, *Introduction to THz wave photonics* (Springer US, 2010).
39. J. Neu and C. A. Schmuttenmaer, "Tutorial: An introduction to terahertz time domain spectroscopy (THz-TDS)," J. Appl. Phys. **124**(23), 231101 (2018).
40. E. Yablonovitch, D. L. Allara, C. C. Chang, T. Gmitter, and T. B. Bright, "Unusually Low Surface-Recombination Velocity on Silicon and Germanium Surfaces," Phys. Rev. Lett. **57**(2), 249–252 (1986).
41. Z. G. Ling and P. K. Ajmera, "Measurement of bulk lifetime and surface recombination velocity by infrared absorption due to pulsed optical excitation," J. Appl. Phys. **69**(1), 519–521 (1991).
42. H. Fischer and O. J. F. Martin, "Engineering the optical response of plasmonic nanoantennas," Opt. Express **16**(12), 9144–9154 (2008).
43. M. A. Ordal, R. J. Bell, R. W. Alexander, L. L. Long, and M. R. Querry, "Optical properties of Au, Ni, and Pb at submillimeter wavelengths," Appl. Opt. **26**(4), 744–752 (1987).
44. E. D. Palik, *Handbook of Optical Constants of Solids* (Academic Press, 1997).
45. F. Meng, M. D. Thomson, B. E. Sernelius, M. Jörger, and H. G. Roskos, "Ultrafast dynamic conductivity and scattering rate saturation of photoexcited charge carriers in silicon investigated with a midinfrared continuum probe," Phys. Rev. B **91**(7), 075201 (2015).
46. L. Gingras, W. Cui, A. W. Schiff-Kearn, J.-M. Ménard, and D. G. Cooke, "Active phase control of terahertz pulses using a dynamic waveguide," Opt. Express **26**(11), 13876–13882 (2018).
47. J. Bühler, J. Allerbeck, G. Fitzky, D. Brida, and A. Leitenstorfer, "Terahertz shockwaves generated by a precise subcycle cut of the electric field," Optica **5**(7), 821–824 (2018).